Available online at www.sciencedirect.com
ScienceDirect
Acta Materialia 57 (2009) 1768–1776
Acta MATERIALIA
www.elsevier.com/locate/actamat

Investigation of fracture properties of magnetron-sputtered TiN films by means of a FIB-based cantilever bending technique

S. Massl [a,*], W. Thomma [a], J. Keckes [b], R. Pippan [a]

[a] Erich Schmid Institute of Materials Science, Austrian Academy of Sciences, Jahnstrasse 12, A-8700 Leoben, Austria
[b] Department Materials Physics, University of Leoben, A-8700 Leoben, Austria

Received 24 July 2008; received in revised form 20 November 2008; accepted 16 December 2008
Available online 23 January 2009

Abstract

A cantilever bending technique for the determination of mode I fracture toughness and strength of thin films is presented. First, the depth profile of residual stresses in the film is determined in order to investigate the possible existence of pronounced stress gradients. Then cantilevers, about 70 μm in length and consisting of the film and the substrate, are fabricated by means of a focused ion beam workstation. The beams are loaded with an in situ microindenter until fracture, which allows the fracture toughness and the strength of the thin film to be calculated from the load–deflection curve and the residual stresses to be determined. The method is presented by investigating the fracture properties of a 1.1-μm thick magnetron-sputtered TiN film on Si, leading to a fracture toughness of 2.6 ± 0.3 MPa $\sqrt{m}$ and a strength of $\sigma_f = 4.4 \pm 0.5$ GPa. Finally, the influence of the compressive residual stresses on the structural integrity and the role of the grain boundary strength are discussed.

Keywords: Thin films; Fracture; Residual stresses; Grain boundaries

1. Introduction

The strength and fracture toughness of thin ceramic films are important material parameters owing to their significant influence on the lifetime and the structural integrity of coated components. Such parameters are usually difficult to measure due to the small dimensions and brittleness of thin films.

To date, there has been no commonly accepted standard testing procedure that allows the reliable, simple and reproducible determination of strength and fracture toughness of ceramic thin films. Techniques like micro- or nanoindentation [1–4] or the scratch test [5–7] are well-established, but the determination of fracture strength and fracture toughness is rather difficult owing to the complex stress fields induced in the material investigated during loading. Furthermore, the results obtained often quantify the apparent fracture behaviour of a particular film–substrate system instead of the parameters of a specific material [8]. This problem has been approached recently by methods like the four-point-bending method [9], the microbridge method [10] or the microtensile fracture technique [11], which feature defined sample and loading geometries and therefore facilitate the calculation of the actual fracture toughness and/or strength of thin films.

The fracture behaviour of thin films on substrates is controlled by mechanical properties, such as the strength and fracture toughness of the film, the strength of the interface and the residual stress in the film. Independent evaluation of these parameters is important to understand the properties of coated systems and to ensure mechanical reliability [8]. In this paper, we focus on the fracture behaviour of the film material itself. As a model system, a 1.1-μm thick TiN film deposited on single crystalline (100) Si by means of physical vapour deposition (PVD) is tested under mode I loading. In general, the strength and fracture toughness of such films are strongly influenced by the structural

* Corresponding author. Tel.: +43 3842 804 214; fax: +43 3842 804 116.
E-mail address: stefan.massl@mu-leoben.at (S. Massl).

1359-6454/$36.00
doi:10.1016/j.actamat.2008.12.018

morphology of the coating, which usually exhibits a columnar structure [1,3,12]. The relative weakness of the grain boundaries compared to the TiN grains leads predominantly to intergranular fracture with the crack propagating perpendicular to the substrate–film interface, as discovered by nanoindentation [1–4] and scratch tests [5]. Some research groups have suggested that the strength of the grain boundaries of PVD-deposited TiN films on steel substrates is so low that in fact the high compressive residual stresses might be the most important factors for the mechanical stability of the film [4,12,13].

The purpose of this paper is to present a new technique for the evaluation of strength and mode I fracture toughness of thin films based on the fabrication of microcantilevers by means of a focused ion beam (FIB) workstation and the subsequent testing of these cantilever beams in an in situ microindenter mounted in a scanning electron microscope (SEM). The advantages as well as the limitations of the method presented, the measured strength and fracture toughness are investigated. Finally, the role of the grain boundary strength and the residual stresses for the mechanical integrity of the coated system are discussed for the presented example.

2. Experimental

A 1.1-μm thin TiN film was deposited onto a 450-μm thick silicon (100) substrate at 550 °C by means of reactive sputtering from a Ti target in an $Ar + N_2$ atmosphere using a laboratory-scale unbalanced DC magnetron-sputtering system. The total pressure and the bias voltage were 0.25 Pa and −50 V, respectively. The thin film was then subjected to a thermal cycle from 25 to 700 °C in vacuum at a maximum pressure of 10^{-3} Pa at a heating and cooling rate of 5 K min^{-1} [14].

The depth profile of residual stresses in the TiN film was determined by means of the ion beam layer removal method (ILR method [15]), which is described briefly here. The ILR method is based on the fabrication of a cantilever by means of a FIB workstation in the vicinity of the specimen edge. In the presented example, a Zeiss XB1540 Crossbeam FIB, which combines a gallium-operated 30 kV FIB and a high-resolution SEM equipped with a field emission gun, was used to fabricate the cantilever consisting of the 1.1-μm thick film and the 5.3-μm thick substrate. The cantilever bends owing to the residual stresses, similar to a bimetallic strip, and the deflection of the free end is measured with the SEM at high magnification. The thin film is then removed gradually in section A, which leads to a change in the curvature of this section owing to the removal of the stressed material, as shown in Fig. 1. By considering the deflection versus film thickness curve, the dimensions of the cantilever and the elastic moduli of the materials involved, the depth profile of the residual stresses in the cantilever and finally in the initial system is determined. In the presented example, the Young's moduli and Poisson's ratios necessary for the calculation of the biaxial Young's moduli were taken from the literature ($E_{Si(100)} = 130$ GPa ± 5%, $\nu_{Si} = 0.28 \pm 0.01\%$ and $E_{TiN} = 309$ GPa ± 24%, $\nu_{TiN} = 0.27 \pm 14\%$ [16–31]). The calculated depth profile of residual stresses in the TiN thin film of the initial system film is shown in Fig. 2. For comparison, the average film stress was determined by means of the well-known wafer curvature technique [32–34], showing good agreement of the results ($\overline{\sigma}_{WCM} = -1.2$ GPa, $\overline{\sigma}_{ILR} = -1.5$ GPa).

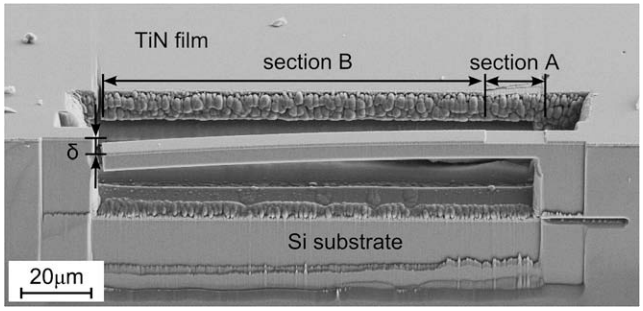

Fig. 1. SEM image of a microcantilever fabricated with a FIB workstation for the determination of a depth profile of residual stresses in a thin film by means of the ILR method (inclined view). The thin film is removed gradually in section A, which affects the residual stresses and therefore the curvature. This change in curvature is amplified by section B, which acts as a curved indicator. The deflection δ as a function of film thickness is the basis for the calculation procedure.

In addition to the microbeam for the determination of the stress profile, eight cantilevers for the actual fracture experiments were fabricated along the Si ⟨100⟩ direction by means of the FIB from the same specimen where the stress distribution was determined as described above. Four of the cantilevers (1–4) were used for the determination of fracture stress in the TiN film; the remaining four

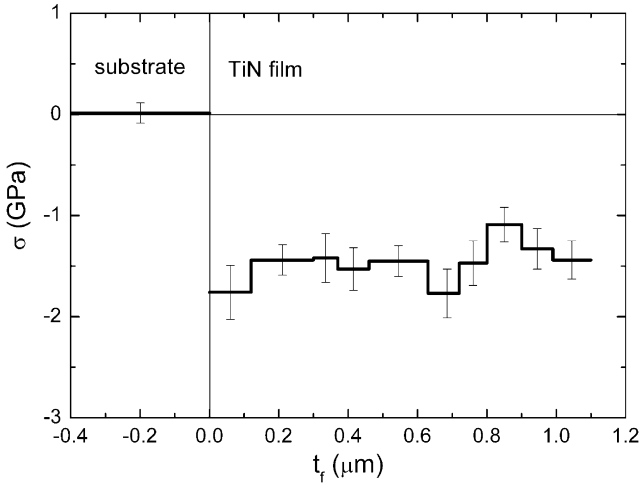

Fig. 2. Depth profile of residual stresses in the TiN film of the initial system determined by means of the ILR method. This film exhibits a homogeneously distributed compressive stress with an average value of −1.5 GPa. The error bars are computed by using the propagation of errors considering the uncertainties in the Young's moduli, the dimensions of the cantilever and the deflections measured.

(5*–8*) were prepared later on to determine the fracture toughness of the film. The cantilever substrate thicknesses ranged from 2 to 10 μm, leading to different residual stress distributions in the microbeams and consequently different deflections, as shown for two examples in Fig. 3.

The experimentally measured deflections δ_{exp} of the eight cantilevers were compared with the corresponding calculated deflections δ_{calc} as listed in Table 1. These deflections were calculated from the depth profile of residual stresses in the initial system determined by means of the ILR method, the elastic constants of the materials involved, the substrate thicknesses of the initial system and the cantilevers, as well as the cantilever lengths, using simple beam theory. In addition to the good agreement of the average film stresses determined by means of the ILR method and the wafer curvature method, as mentioned above, the excellent correspondence between the experimentally measured and the calculated deflections indicates the reliability of the depth distribution of residual stresses determined for the thin film.

The fabrication of a number of cantilevers of different thickness furthermore offers the possibility of investigating the reliability of the fracture properties determined for the thin film. The basic idea behind this check is that the values for the strength and for the fracture toughness should be independent of the substrate thickness of the cantilever investigated because they are fabricated from the same coated system. If the values calculated from cantilevers with different substrate thicknesses do not scatter significantly, pronounced effects of substrate thickness on the fracture properties determined can be excluded. Furthermore, the experiments for the determination of the strength are simulated by means of the finite element analysis software Abaqus version 6.7 to account for the changes in the stress state in the vicinity of the origin at the cantilever surface.

Table 1
Dimensions, as well as experimentally determined and calculated deflections, of the cantilever curving owing to the residual stresses.

Cant No.	l (μm)	w (μm)	t_{sub} (μm)	δ_{exp} (μm)	δ_{calc} (μm)
1	64.5	9.6	8.7	0.74	0.68
2	64	10	5.3	1.4	1.31
3	72	10.5	4.8	1.9	1.87
4	67	9.8	2	3.4	3.95
5*	68	10	10	0.74	0.61
6*	60	10	6.5	1.0	0.88
7*	77	10.8	5	2.0	2.04
8*	65	10.6	2.2	3.2	3.44

The comparison of the deflections shows excellent correlation. The asterisks indicate the cantilevers for the determination of the fracture toughness that are provided with a pre-crack after the comparison of the deflections.

In order to facilitate the description of the stresses in this region, the p-axis, with its origin lying at the cantilever origin, is introduced, as shown in Fig. 4(a). The positions where the surface stresses in the direction of the p-axis were investigated in detail range from $p = -2$ μm to $p = +2$ μm in steps of 1 μm. The two cantilevers with the largest and the smallest substrate thickness $t_{sub,c1} = 8.7$ μm and $t_{sub,c4} = 2$ μm) were simulated using 4-node bilinear elements of the type CPE4I. These simulations took into account that the width of cantilever changes not directly at the origin ($p = 0$) but a few microns in the negative p-direction, as shown in Fig. 4, which is an important measure to reduce the complexity of the stresses at the cantilever origin.

After fabricating the cantilevers and measuring the deflections, tungsten marks of about 2 μm length, 500 nm

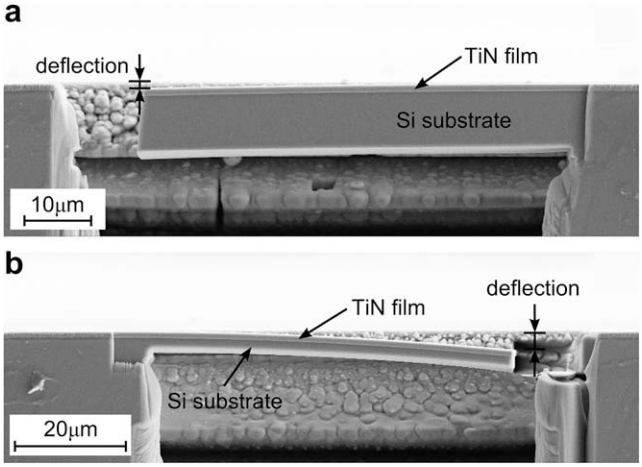

Fig. 3. SEM images of FIB-fabricated cantilevers used for the fracture experiments (front view). The cantilevers deflect owing to the intrinsic residual stresses, which depend on the substrate thickness, among other things. Cantilever 1, shown in (a), has a substrate thickness of 8.7 μm and exhibits a downward deflection of 0.74 μm, whereas the substrate of cantilever 8* (b) is only 2.2 μm thick, resulting in a downward deflection of 3.2 μm. It should be emphasized that the deflection of cantilever 8* was measured before introducing the pre-crack.

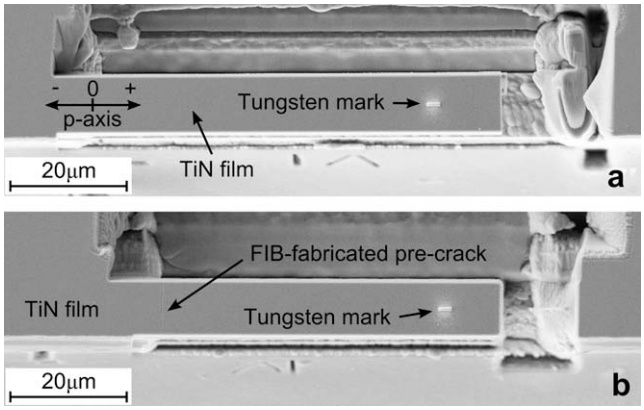

Fig. 4. SEM images of cantilevers for fracture experiments (top view). The cantilevers without a pre-crack, shown in (a), are used for the determination of the fracture strength, whereas the FIB-notched cantilever beams, shown in (b), allow the determination of the fracture toughness of the thin film. The bright spots near the free end of the cantilever are the FIB-deposited tungsten marks. The p-axis is introduced in order to facilitate the description of the stresses at the surface in the vicinity of the cantilever origin.

width and 500 nm height were deposited on the thin film near the free ends in the mirror plane of the cantilevers by means of the gas injection system attached to the FIB workstation, as shown in Fig. 4. These marks facilitate the location of the exact center of the beam with the in situ microindenter. Then 200 nm deep pre-cracks were introduced in the vicinity of the origin of the four cantilevers fabricated for the determination of the fracture toughness. The location of the pre-cracks about 1 μm away from the origin in the positive *p*-direction minimizes the influence of the abrupt change in substrate thickness on the stresses at the origin. The pre-crack was fabricated by means of the FIB with an ion current of 50 pA to ensure a defined pre-crack and to reduce the ion damage. The milling time was adjusted to the cantilever width to obtain pre-cracks of uniform depth. High-magnification SEM images show a notch radius of the FIB-fabricated pre-cracks of 10 nm, as shown in Fig. 5. The influence of the notch radius on the fracture toughness was estimated later on using an approach based on the simultaneous application of energy and stress fracture criteria introduced by Picard et al. [35].

The actual fracture mechanical tests were performed by means of an ASMEC UNAT in situ microindenter equipped with a cube corner tip mounted in a Zeiss 440 SEM. First, the cantilever to be tested was positioned in the vicinity of the indenter. The sample was mounted in the SEM in such a way that a front view of the cantilever was obtained, which allowed only coarse positioning of the specimen in the *z*-direction, as shown in Fig. 6. To position the indenter tip exactly in the mirror plane of the cantilever, the tip is lowered slowly onto the FIB-deposited tungsten marks. At the desired *z*-position of the sample, the tip touches the top of the mark and the measured force increases slightly; otherwise, the tip would disappear

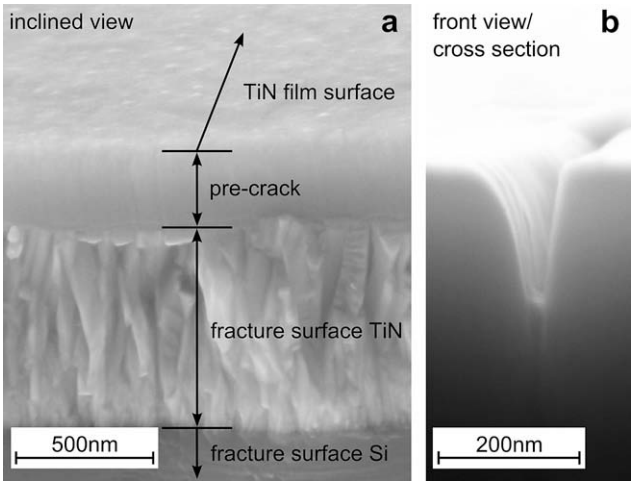

Fig. 5. SEM images of the fracture surface of a notched cantilever and the FIB-fabricated pre-crack. The inclined view on the fracture surface in (a) shows the approximate dimensions of the pre-crack, inhomogeneities in the notch root where stress concentrations could occur during loading and the predominantly intergranular fracture appearance. The exact shape of the pre-crack is shown in (b).

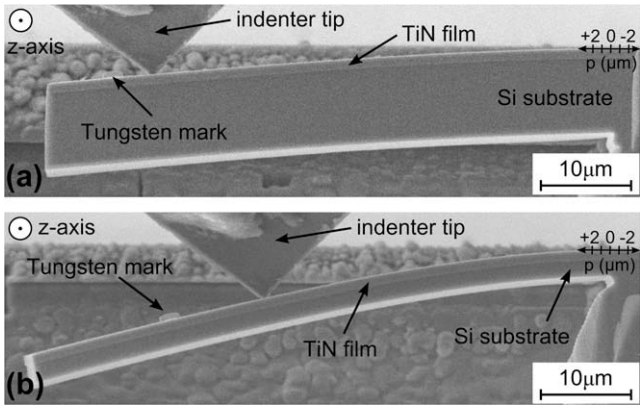

Fig. 6. SEM pictures of the loading of cantilever 1(a) and cantilever 4(b), both without a pre-crack, by means of the in situ microindenter just before fracture (front view). Cantilever 4 sustains a larger curvature than cantilever 1 owing to the difference in substrate thickness. Nevertheless, the fracture stresses along the *p*-axis at the film surface resulting from superimposing the residual stresses and the stresses induced by the loading are very similar.

behind the tungsten mark, or vice versa, and the *z*-position would have to be adjusted. Now the stage is moved to position the indenter tip a few microns away from the free end of the cantilever for the actual experiment. On one hand, a large distance between the origin of the cantilever and the tip is necessary to ensure that the bending load is predominantly at the origin and to minimize the shear stresses. On the other hand, the tip must be located at a safe distance from the free end of the cantilever to avoid shearing off the thin film. This is especially important for the thin cantilevers, where large deflections were obtained during the experiments. The distances between the loading point and the cantilever origin ranged between 37.9 μm for cantilever 8* and 53.8 μm for cantilever 7*, as listed in Table 2, which produced convenient ratios between the maximum normal and the shear stresses. The cantilever was load–displacement controlled with 2.5 nm s^{-1}, as shown in Fig. 6, and the load–deflection curve was recorded. SEM images were recorded every 60 s to survey the experiment.

In addition to the actual fracture experiments, the specimen was indented far away from the FIB-fabricated canti-

Table 2
Deflection, load at fracture and loading distances for the cantilevers tested.

Cant No.	d_{frac} (μm)	F_{frac} (mN)	l_{load} (μm)
1	3.51	8.13	50.5
2	3.86	4.41	42.7
3	4.85	4.26	48.6
4	4.85	1.47	38.8
5*	2.73	10.05	48.3
6*	2.69	5.77	40.6
7*	4.62	3.38	53.8
8*	3.4	1.16	37.9

The pre-cracked cantilevers for the determination of the fracture toughness are marked with an asterisk.

levers with the same loading parameters. This allowed the load–deflection curve recorded during the cantilever fracture experiments to be separated into a contribution coming from the actual bending of the cantilever and a contribution resulting from the indentation into the thin film. In other words, the corrected curve describes the force necessary to deflect an impenetrable cantilever. The determination of the corrected load–deflection curves is essential because, especially in the case of cantilevers with thick substrates, the deflection values of the as-recorded curves overestimate the actual deflection of the cantilever due to the formation of the imprint.

3. Results

The as-recorded as well as the corrected load–deflection curves showed perfect linear behaviour until fracture for all the cantilevers tested, as shown in Fig. 7 for cantilever 1 (without pre-crack), for example. Owing to the substrate thickness of 8.7 μm, this cantilever was relatively stiff, which led to a significant penetration of the indenter tip and therefore a noticeable difference between the two curves. The corrected load–deflection curves of all eight cantilevers tested are shown in Fig. 8. The deflections resulting from loading, the loads at fracture and the corresponding deflections as well as the loading distances between the indenter tip and the cantilever origins are listed in Table 2. The investigation of the fractured cantilever shows that the pre-cracked cantilevers fractured exactly at the FIB-fabricated pre-crack, whereas the cantilevers without notch failed in the immediate vicinity of the cantilever origin, as shown in Fig. 9. In latter case, cantilevers 2, 3 and 4 failed in the vicinity of the origin in the positive *p*-direction; the thickest cantilever, cantilever 1, fractured close to the origin in the negative *p*-direction.

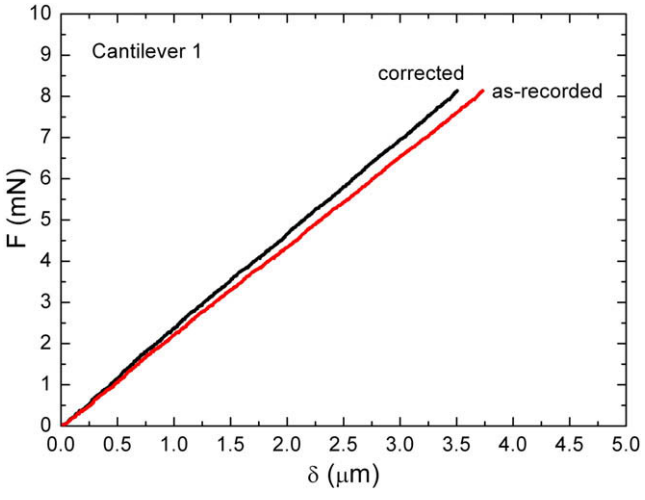

Fig. 7. As-recorded and corrected load–deflection curve for cantilever 1. The corrected curve describes solely the force necessary to deflect the cantilever, whereas the as-recorded curve additionally considers the contribution of the penetration of the indenter tip into the thin film. This contribution can be neglected in the case of cantilevers with thin substrates, where only small forces are necessary to produce a certain amount of bending, which leads to shallow indents.

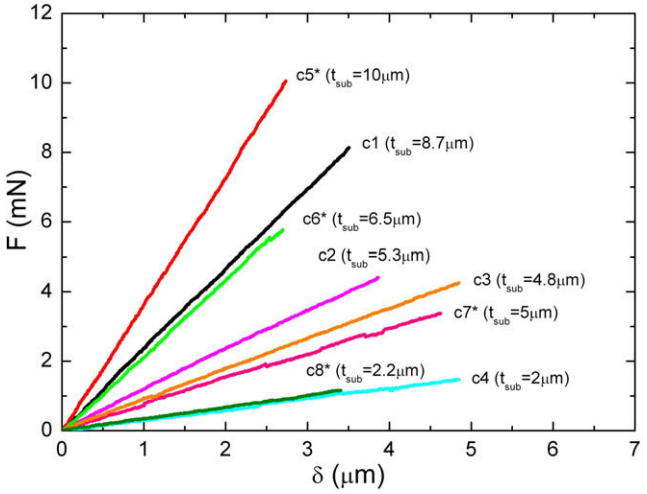

Fig. 8. Corrected load–deflection curves of the cantilevers examined. Although general trends can be seen, it must be taken into account that the curves cannot be compared directly because of the differences in widths and loading distances. Nevertheless, all cantilevers tested show perfectly linear load–deflection curves until fracture. The pre-cracked cantilevers are marked with an asterisk.

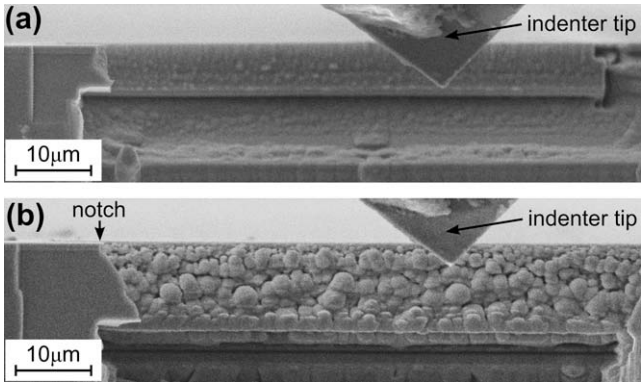

Fig. 9. SEM images of fractured cantilevers (front view). The cracks in the cantilevers without a pre-crack initiated and propagated in the vicinity of, but not exactly at, the origin of the beam, as shown in (a) for cantilever 3, whereas notched cantilevers fracture exactly at the pre-crack, as shown for cantilever 5* in (b).

The fracture stress of the TiN film was determined from the cantilevers without pre-cracks by superimposing the residual stress profiles resulting from the intrinsic stresses and the stresses at the origin of the cantilever induced by the loading. The crack was assumed to form at the surface where the tensile stresses are highest. Therefore, the fracture stress is simply the surface stress in the cantilever direction at its origin just before fracture. The validity of this simple consideration of the surface stresses in the immediate vicinity of the cantilever origin just before fracture was confirmed by means of finite element simulations, as mentioned above. The results listed in Table 3 show that, in the case of cantilever 1 $t_{sub,c1} = 8.7$ μm), the stresses do

Table 3
Stresses in the vicinity of the origins of the cantilevers 1 and 4 just before fracture obtained by finite element simulations, taking into account the intrinsic residual stresses and the stresses induced by the loading with the microindenter.

Cant No.	$\sigma_{p=2}$ (GPa)	$\sigma_{p=1}$ (GPa)	$\sigma_{p=0}$ (GPa)	$\sigma_{p=-1}$ (GPa)	$\sigma_{p=-2}$ (GPa)
1	4.03	3.98	3.79	3.65	3.37
4	5.43	5.54	5.13	4.08	2.73

The values for the positions along the p-axis are given in microns.

not vary significantly around the origin, whereas in the case of cantilever 4 ($t_{sub,c4} = 2\mu m$) the stresses also stay almost constant in the positive p-direction and drop significantly in the negative p-direction.

The fracture toughness of the TiN film was determined from the experiments carried out with the pre-cracked cantilevers. As described above, first the intrinsic stresses and the stresses at the cantilever's origin owing to loading were superimposed. Then the stresses in the length direction 200 nm below the surface, which is the exact location of the crack tip, were calculated. These stresses were approximated well by a stress profile resulting from a bending moment applied at the tip of the cantilever because the stresses at the origin of the cantilever are mainly a result of the external loading. This moment was calculated in such a way that it produced the same stress 200 nm below the surface as the combination of the residual stresses and the loading. The advantage of this simplification is that there is an existing numerical solution for the calculation of the fracture toughness for a pre-cracked bimaterial beam subjected to a bending moment [36].

As mentioned above, the influence of the root radius of the FIB-fabricated pre-crack was estimated by means of a method developed by Picard et al. that allows the determination of a corrected value of the fracture toughness taking into account the root radius and the fracture toughness measured, as well as the strength of the material investigated. Using the average values for the fracture toughness and the strength determined ($2.6 MPa\sqrt{m}$ and 4.4 GPa, respectively) as well as the SEM-measured notch radius of 10 nm, a value for the fracture toughness of 2.5 MPa $\sqrt{m}$ was calculated with this technique. The negligible difference between the experimentally determined value and this corrected value led us to conclude that the root radius is small enough to consider the pre-crack as ideally sharp.

The individual values for the strength and fracture toughness of the TiN film determined as a function of the cantilever substrate thickness are listed in Table 4.

Table 4
Summarized results of the strengths and the fracture toughnesses of the TiN film determined, together with the corresponding cantilever substrate thicknesses.

Cant No.	t_{sub} (μm)	σ_f (GPa)	K_{Ic} (MPa $\sqrt{m}$)
1	8.7	3.79 ± 0.44	–
2	5.3	3.78 ± 0.43	–
3	4.8	4.73 ± 0.53	–
4	2	5.13 ± 0.70	–
5*	10	–	2.63 ± 0.32
6*	6.5	–	2.61 ± 0.27
7*	5	–	2.87 ± 0.28
8*	2.2	–	2.22 ± 0.25

4. Discussion

The method presented allows a straightforward, local and reliable determination of fracture toughness and fracture stress of brittle thin films owing to the defined stress state in the region of interest resulting from the sample and loading geometry. As a prerequisite, it is important to evaluate the depth profile of residual stresses in the coating prior to the actual fracture experiments by means of either the ILR method [15], as in this paper, or other techniques, based on Raman spectroscopy [37–40] or grazing incidence X-ray diffraction [41–44], for example. In the case of pronounced stress gradients, the simple determination of the average stresses could lead to an over- or underestimation of the stresses in the region of interest.

The method can be applied to a wide range of thin film/substrate material combinations, but it should be taken into account that, in the case of plastic deformation occurring during the experiment, the determination of the fracture mechanical parameters will become more complex and may need to involve further finite elements simulations. If possible, materials sensitive to ion damage should not be investigated with a FIB operated with an acceleration voltage of 30 kV, as presented here. Instead, the FIB ought to be operated with a lower acceleration voltage or lower ion energies. The implantation depth of the accelerated ions can be estimated by performing an SRIM (stopping and range of ions in matter [45]) simulation. Materials like aluminium, for example, that exhibit pronounced Ga-induced grain boundary embrittlement should not be investigated in a Ga-operated FIB.

The average fracture toughness and strength determined were 2.6 ± 0.3 MPa $\sqrt{m}$ and 4.4 ± 0.5 GPa, respectively. The uniformity of the results shows that the cantilever substrate thickness and therefore the depth profile of residual stresses in the curved cantilever does not influence these values significantly. The stresses in the region of interest – at the surface or in front of the FIB-fabricated pre-crack, respectively – depend solely on the superposition of the intrinsic stresses in the curved cantilever and the stresses induced by the loading, as expected according to basic mechanics.

The finite element simulation of the stresses in the vicinities of the origins of the unnotched cantilevers shows that these stresses do not vary significantly even 2 μm away from the origin in the case of a thick substrate, as listed in Table 3. This simulation led us to conclude that the probability of the fracture is equally distributed in this region taking into account only the stresses. Certainly,

the actual initiation of the fracture process is controlled by atomistic flaws of critical size or larger located near the surface of the thin film. This consideration is supported experimentally by the fact that cantilever 1 ($t_{sub,c1} = 8.7$ μm) fractured about 2 μm away from the origin in the negative p-direction. The corresponding simulation for the thinnest cantilever 4 ($t_{sub,c4} = 2\mu m$) shows that the surface stresses decrease significantly in the negative p-direction and increase slightly in the positive p-direction, which suggests an initiation of fracture at $p \geqslant 0$ μm. As proposed by this simulation, cantilevers 2, 3 and 4 fractured between 2.4 and 3.2 μm away from the origin in the positive p-direction.

The mode I fracture toughness determined was confirmed by the method developed by Picard et al. [35], which also showed that the root radius of the FIB-fabricated pre-crack of 10 nm was small enough to ensure that the experiments were valid. Furthermore, the front of the pre-crack was not perfectly straight owing to the FIB milling process, as shown in Fig. 5(a). This could lead to critical local stress concentrations even at low loads and consequently to local atomically sharp cracks in the root that subsequently act as ideal pre-cracks.

Another important factor that has to be considered for such fracture mechanical investigations is the microstructure of the thin film, which can influence the fracture behaviour significantly [12]. On one hand, the independence of the values determined on the stress distribution in the TiN film clearly indicates that the fracture properties of the film itself are not affected by the residual stresses, but rather by the strength and fracture toughness of the grains and the grain boundaries, which depends mainly on the deposition process and parameters. On the other hand, residual stresses are definitely important for the structural integrity of coated components because high compressive stresses hinder crack nucleation and propagation in the coating, even if the resistance against fracture of the thin film itself is low. Therefore, the most important task is to produce films which exhibit high compressive residual stresses, good fracture properties and sufficient adhesion to the substrate material in order to prevent failure.

A challenging task was to compare our results with those obtained by other research groups, because there are virtually no reports in the literature to compare the fracture toughness and strength with. Kamiya et al. [8,46] investigated the fracture mechanical parameters of 4 and 7 μm thick PVD-deposited TiN films deposited on WC–Co cutting inserts by means of a combination of microfracture tests and simulations. The critical energy release rates were between 21.2 J/m^2 for the 4 μm and 16.4 J/m^2 for the 7 μm thick film, corresponding to critical stress intensity factors of 2.7 MPa $\sqrt{m}$ and 2.3 MPa $\sqrt{m}$, respectively, considering the plane strain state in front of the crack tip, the Young's modulus of TiN used for the ILR method $E_{TiN} = E_{biax,TiN} \cdot (1 - \nu_{TiN}) = 309$ GPa) and Eq. (1):

$$K_c = \sqrt{\frac{E \cdot G_c}{1 - \nu^2}} \tag{1}$$

Although their experimental setup, the substrate material and the deposition conditions were different from ours, both values determined by Kamiya et al. correspond well to the mode I fracture toughness of 2.6 ± 0.3 MPa $\sqrt{m}$ presented here.

Kamiya et al. [8] also evaluated the strength of free-standing thin film cantilevers of approximately 100 μm length and 50 μm width by bending the cantilever beams by means of a loading device and measuring the load at fracture. When they bent the cantilever downwards, the crack initiated near the surface, similar to the experiment presented here. Nevertheless, the strength of the TiN film obtained by means of that method was 2.6 GPa, which is significantly lower than the result determined in this paper ($\sigma_f = 4.4 \pm 0.5$ GPa). It should be mentioned that Kamiya et al. [8] analyzed the strength of the brittle film using the well-known Weibull distribution in order to account for the cantilever size and the possibility of atomistic flaws of critical size being located in the cantilever beam owing to the deposition process.

Qin et al. [47] investigated the strength of 2 μm thick multi-arc ion plated TiN films deposited on steel by straining the substrate and calculating the stress of the film by means of X-ray diffraction. The fracture strength determined was 7.01 GPa, which is significantly higher than the result presented here. The comparison of the strength of the ion-plated coatings [8,46,47] and the magnetron-sputtered TiN film investigated in this paper shows that the values scatter significantly, presumably as a result of the deposition techniques and parameters.

More information about the initiation and propagation of the cracks in the TiN film can be obtained by analyzing the stresses in the cantilevers and the fracture surfaces. For this purpose, the cantilever beams without pre-cracks used for the determination of the film strength were investigated in detail because the stresses are more defined than in the case of the pre-cracked specimens and the crack initiation process can be discussed. The first issue to be analyzed is whether the crack initiates at the surface of the cantilever, where the stresses are highest in the TiN film, or at the interface in the Si, where the tensile stresses in the substrate are highest. Another location of the starting point of the crack in the thin film is very unlikely owing to the pronounced stress gradient induced by the loading with the indenter. Also, the investigation of the stresses just before fracture showed that all the cantilevers failed at similar film stresses at the surface, as listed in Table 4, but at different maximum substrate stresses ($\sigma_{Si,max} = 1.8GPa$, $\sigma_{Si,min} = 0.7GPa$) owing to the variation in cantilever substrate thicknesses ($t_{sub,max} = 8.7$ μm, $t_{sub,min} = 2\mu m$), which led us to conclude that the cracks originated at the surface. For comparison, the stress profiles of two loaded cantilevers of different substrate thicknesses are shown in Fig. 10. A critical flaw size of $a_c = 108$ nm, which is somewhat larger than the width of the columnar grains, was roughly estimated by applying the well-known Griffith's criterion

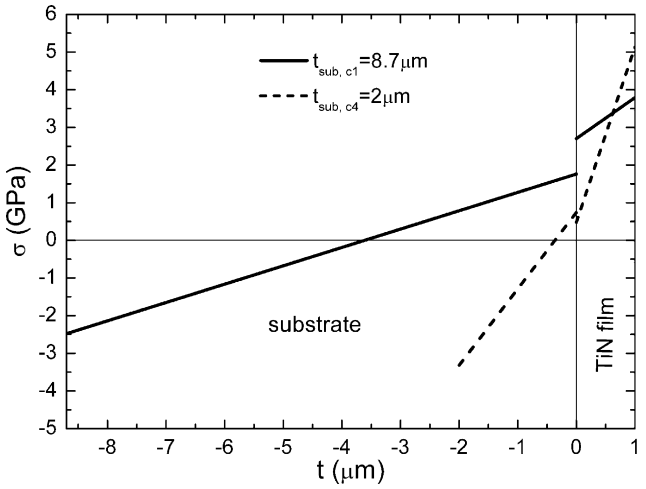

Fig. 10. Stress profiles just before fracture in two cantilevers (1 and 4) without a pre-crack, but of different substrate thickness. These depth profiles develop by superimposing the intrinsic residual stresses and the stresses induced by the loading. In this graph, the nearly homogeneously distributed stresses in the initial system shown in Fig. 2 are approximated by a perfectly homogeneous stress profile with the same average stress.

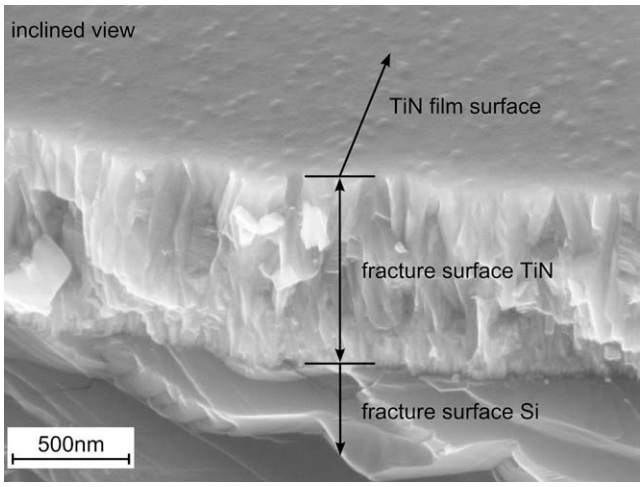

Fig. 11. SEM image of a fracture surface of the TiN film investigated shows mainly intergranular fracture (inclined view).

(Eq. (2)), considering the mode I stress intensity factor and the strength of the TiN film determined in this paper.

$$a_c = \frac{1}{\pi}\left(\frac{K_{Ic}}{\sigma_f}\right)^2 \tag{2}$$

The SEM images of the fracture surface show that intergranular cleavage is the dominant fracture mechanism of the film, which has also been reported for other TiN coatings by other research groups [1–4,12]. Examples of the fracture surfaces of the TiN film investigated are shown in Figs. 5(a) and 11.

The results obtained demonstrate that the TiN thin film can sustain significant tensile stresses, which is contrary to the assumption that the compressive stresses in the coating are the most important point to assure the integrity of the system [4,12,13]. Owing to the observed intergranular fracture, the strength measured is actually the strength of the grain boundaries. The combination of relatively high fracture toughness, high strength, compressive stresses in the TiN film on the substrate and sufficient adhesion is responsible for the good mechanical performance of the system investigated. However, it has to be taken into account that the quality (defect density, homogeneity, etc.) and the properties of a film depend strongly on the fabrication process and the deposition parameters, and it is therefore difficult to draw conclusions about TiN films in general.

5. Conclusion

The results demonstrate that the method presented here is a powerful tool for the determination of the mode I fracture toughness and the intrinsic strength of thin films. The defined stress state in the region of interest during loading and the straightforward calculation procedure led to reliable and reproducible results, as shown by means of the PVD-deposited TiN film on single crystalline Si. The fracture toughness of 2.6 ± 0.3 MPa $\sqrt{m}$ corresponds well to results obtained by Kamiya et al. [46]. The strength of $\sigma_f = 4.4 \pm 0.5$ GPa is surprisingly high, although values up to 7.01 GPa have been reported for PVD-deposited TiN films [47]. SEM images reveal that intergranular cleavage is the dominant fracture mechanism. These results lead to the conclusion that the structural integrity of the film results mainly from the high grain boundary strength rather than from simply high compressive stresses.

Acknowledgements

The authors thank the Austrian Science Foundation FWF for supporting this work and M. Swain, R. Schöngrundner, K.J. Martinschitz, H. Köstenbauer and S. Roberts for helpful discussions.

References

[1] Weppelmann E, Swain MV. Thin Solid Films 1996;286:111.
[2] Ma LW, Cairney JM, Hoffman M, Munroe PR. Surf Coat Technol 2005;192:11.
[3] Bhowmick S, Xie ZH, Hoffman M, Jayaram V, Biswas SK. J Mater Res 2004;19:2616.
[4] Xie ZH, Hoffman M, Moon RJ, Munroe PR. J Mater Res 2006;21:437.
[5] Xie ZH, Hoffman M, Munroe P, Singh R, Benadavid A, Martin PJ. J Mater Res 2007;22:2312.
[6] Kim KH, Han D-S, Kim SK. Surf Coat Technol 2003;163-164:605.
[7] Ichimura H, Ishii Y. Surf Coat Technol 2003;165:1.
[8] Kamiya S, Hanyu H, Amaki S, Yanase H. Surf Coat Technol 2007;202:1154.
[9] Jaeger G, Endler I, Heilmaier M, Bartsch K, Leonhardt A. Thin Solid Films 2000;377–378:382.
[10] Zhang TY, Su YJ, Qian CF, Zhao MH, Chen LQ. Acta Mater 2000;48:2843.
[11] Jonnalagadda K, Cho SW, Chasiotis I, Friedmann T, Sullivan J. J Mech Phys Solids 2008;56:388.
[12] Bhowmick S, Jayaram V, Biswas Sk. Acta Mater 2005;53:2459.

[13] Jayaram V, Bhowmick S, Xie ZH, Math S, Hoffman M, Biswas SK. Mater Sci Eng A 2006;423:8.
[14] Köstenbauer H, Fontalvo GA, Kapp M, Keckes J, Mitterer C. Surf Coat Technol 2007;201:4777.
[15] Massl S, Keckes J, Pippan R. Acta Mater 2007;55:4835.
[16] Freund LB, Suresh S, Thin film materials. Cambridge: Cambridge University Press; 2003, p. 244.
[17] Mendibide C, Steyer P, Esnouf C, Goudenau P, Thiaudiere D, Gailhanou M, Fontane J. Surf Coat Technol 2005;200:165.
[18] Kitamura T, Hirakata H, Itsuji T. Eng Fract Mech 2003;70:2089.
[19] An J, Zhang QY. Surf Coat Technol 2005;200:2451.
[20] Barshilia HC, Deepthi B, Prabhu ASA, Rajam KS. Surf Coat Technol 2006;201:329.
[21] Bedell SW, Reznicek A, Fogel K, Ott J, Sadana DK. Mater Sci Semicon Proc 2006;9:423.
[22] Carlotti G, Doucet L, Dupeux M. Thin Solid Films 1997;296:102.
[23] Novotna Z, Kralova R, Novak R, Marek J. Surf Coat Technol 1999;116-119:424.
[24] Comins JD, Pang W, Every AG, Pietersen D. Refract Met Hard Mater 1998;16:389.
[25] Haider J, Rahman M, Corcoran B, Hashmi MSJ. Mater Proc Technol 2005;168:36.
[26] Bamber MJ, Cooke KE, Mann AB, Derby B. Thin Solid Films 2001;398–399:299.
[27] Kim SH. Mater Lett 2007;16:3589.
[28] Huang Z, Leighton G, Wright R, Duval F, Chung HC, Kirby P, et al. Sens Actuators A 2007;135:660.
[29] Zhang J. J Mater Proc Technol 2002;123:329.
[30] Antunes JM, Fernandes JV, Sakharova NA, Oliveira MC, Menezes LF. Int J Solids Struct 2007;44:8313.
[31] Tran MD, Poublan J, Dautzenberg JH. Thin Solid Films 1997;308–309:310.
[32] Eiper E, Martinschitz KJ, Keckes J. Powder Differ 2006;21:25.
[33] Resnik D, Aljancic U, Vrtacnik D, Mozek M, Amon S. Vacuum 2005;80:236.
[34] Dieing T, Usher BF. Phys Rev B 2003;67:054108.
[35] Picard D, Leguillon D, Putot C. J Eur Cer Soc 2006;26:1421.
[36] Murakami Y. Stress Intensity Factors Handbook, Vol 4. Oxford: Pergamon Press; 2001. pp. 111.
[37] Grabner L. J Appl Phys 1978;49:580.
[38] Dietrich B, Dombrowski KF. J Raman Spectr 1999;30:893.
[39] De Wolf I. J Raman Spectr 1999;30:877.
[40] Atkinson A, Jain SC. J Raman Spectr 1999;30:885.
[41] Genzel C. Mater Sci Technol 2005;21:10.
[42] Marques MJ, Pina J, Dias AM, Lebrun JL, Feugeas J. Surf Coat Technol 2005;195:8.
[43] Ma CH, Huang JH, Chen H. Thin Solid Films 2002;418:73.
[44] Noyan IC, Cohen JB. Residual stress. New York: Springer; 1987.
[45] Ziegler JF, Biersack JP, Littmark U. The stopping range of ions in matter. New York: Pergamon Press; 1985, p. 321.
[46] Kamiya S, Nagasawa H, Yamanobe K, Saka M. Thin Solid Film 2005;473:123.
[47] Qin M, Ju DY, Wu YN, Sun C, Li JB. Mater Charact 2006;56:208.